Carbohydrate Polymers 75 (2009) 472–478

Contents lists available at ScienceDirect

Carbohydrate Polymers

journal homepage: www.elsevier.com/locate/carbpol

Preparation and properties of glycerol plasticized-pea starch/zinc oxide-starch bionanocomposites

Xiaofei Ma [a], Peter R. Chang [b,c,*], Jingwen Yang [a], Jiugao Yu [a]

[a] School of Science, Tianjin University, Tianjin 300072, China
[b] Bioproducts and Bioprocesses National Science Program, Agriculture and Agri-Food Canada, 107 Science Place, Saskatoon, SK, Canada S7N 0X2
[c] Department of Agricultural and Bioresource Engineering, University of Saskatchewan, Saskatoon, SK, Canada S7N 5A9

ARTICLE INFO

Article history:
Received 24 July 2008
Received in revised form 5 August 2008
Accepted 7 August 2008
Available online 15 August 2008

Keywords:
Nanocomposites
Starch
Zinc oxide

ABSTRACT

A bionanocomposite was cast using ZnO nanoparticles stabilized by soluble starch (nano-ZnO) as filler in a glycerol plasticized-pea starch (GPS) matrix. According to the characterization of nano-ZnO particles by Fourier-transform infrared spectroscopy (FT-IR), thermogravimetric analysis (TG) and transmission electron microscopy (TEM), ZnO nanoparitlces (70 wt%) were encapsulated by starch (30 wt%) in nano-ZnO particles of about 10 nm. In GPS/nano-ZnO nanocomposites, loading a low level of nano-ZnO particles improved the pasting viscosity, storage modulus, glass transition temperature and UV absorbance. When the nano-ZnO content varied from 0 to 4 wt%, the tensile yield strength and Young's modulus increased from 3.94 to 10.80 MPa and from 49.80 to 137.00 MPa, respectively. The water vapor permeability decreased from 4.76×10^{-10} to 2.18×10^{-10} g m^{-1} s^{-1} Pa^{-1}. The improvement in these properties may be attributed to the interaction between the nano-ZnO filler and GPS matrix.

1. Introduction

Bionanocomposites, a new generation of nanocomposite materials, signify an emerging field in the frontiers of materials science, life science, and nanotechnology (Darder, Aranda, & Ruiz-Hitzky, 2007). Bionanocomposites are composed of a natural polymer matrix and an organic/inorganic filler with at least one dimension on the nanometer scale. Currently, effort is being focused on the development of natural polymer-based nanocomposites with mechanical and thermal properties, and in some cases, functional properties, enhanced due to either the biological matrix or filler. In addition to these characteristics, bionanocomposites show the remarkable advantages of biodegradability and biocompatibility in various medical, agricultural, drug release and packaging applications (Mangiacapra, Gorrasi, Sorrentino, & Vittoria, 2006).

Among natural polymers, starch is one of the most promising biodegradable materials because it is a renewable resource that is universally available and of low cost. A number of researchers have presented work in the field of starch-based bionanocomposites, which can be obtained by filling a thermoplastic starch matrix with nanofillers such as layer silicates, carbon nanotubes, carbon black, cellulose and starch nanocrystals. Montmorillonite (Huang, Yu, & Ma, 2006; Kampeerapappun, Aht-Ong, Pentrakoon, & Srikulkit, 2007) and kaolinite (Zhao, Wang, & Li, 2008) are the usual layer silicates used in starch-based bionanocomposites. These layer silicates are modified as inorganic nanofillers forming intercalation or exfoliation compounds (Huang, Yu, & Ma, 2005; Ma, Yu, & Wang, 2007; Park, Lee, & Park, 2003), which have a reinforcing effect in the thermoplastic starch matrix, resulting in improved mechanical properties. Glycerol plasticized-starch (GPS)/multiwall carbon nanotube composites are prepared in aqueous solutions and cast as films (Bonnet, Albertini, & Bizot, 2007; Cao, Chen, & Chang, 2007; Ma, Yu, & Wang, 2008). Electrically conductive GPS/carbon black (CB) composites are prepared using an ameliorated casting method and microwave radiation (Ma, Chang, & Yu, 2008). The influence of CB and plasticizer content on the morphology and the electrical conductance of GPS/CB composite have been investigated. Other fillers, such as polysaccharide nanocrystals, have also been studied. Cellulose nanocrystals, prepared from acid hydrolyzed ramie and hemp fibers, have been used as filler to reinforce GPS (Cao, Chen, Chang, Stumborg, & Huneault, 2008; Lu, Weng, & Cao, 2006). Tunicin-whiskers of slender parallelepiped rods with a high aspect ratio were used in the preparation of nanocomposites (Mathew & Dufresne, 2002). Waxy maize starch nanocrystals, obtained by hydrolysis of native granules, have also been used as reinforcing filler in a thermoplastic waxy maize starch matrix plasticized with glycerol (Angellier, Molina-Boisseau, & Dole, 2006).

Zinc oxide (ZnO), an n-type semiconductor, is a very interesting multifunctional material because of its promising application in

* Corresponding author. Address: Bioproducts and Bioprocesses National Science Program, Agriculture and Agri-Food Canada, 107 Science Place, Saskatoon, SK, Canada S7N 0X2. Tel.: +1 306 9567637; fax: +1 306 9567247.
E-mail address: changp@agr.gc.ca (P.R. Chang).

0144-8617/$ - see front matter Crown Copyright © 2008 Published by Elsevier Ltd. All rights reserved.
doi:10.1016/j.carbpol.2008.08.007

solar cells, sensors, displays, gas sensors, varistors, piezoelectric devices, electro-acoustic transducers, photodiodes, UV light emitting devices and antibacterial materials (Chandramouleeswaran et al., 2007). Vigneshwaran et al. (Vigneshwaran, Kumar, & Kathe, 2006) have developed a method to synthesize nano-ZnO particles using water as the solvent and soluble starch as the stabilizing agent. In this paper, ZnO-starch (nano-ZnO) particles were used as filler in the preparation of glycerol plasticized-pea starch (GPS)/nano-ZnO composites. This work focused on the processing of these bionanocomposites and characterization in terms of morphology, pasting properties, dynamic mechanical thermal analysis, mechanical and optical properties, and water vapor permeability (WVP).

2. Experimental

2.1. Materials

Pea starch composed of 35% amylose and 65% amylopectin was supplied by Nutri-pea Limited (Portage la Prairie, Canada). Soluble starch was obtained from Tianjin Fine Chemical Institute (Tianjin, China). Glycerol, bulk zinc oxide, zinc nitrate hexahydrate and sodium hydroxide were of analytical grade from Tianjin Chemical Reagent Factory (Tianjin, China).

2.2. Preparation of nano-ZnO

Nano-ZnO was produced based on the method of Vigneshwaran et al. (Vigneshwaran et al., 2006) with some modifications. 1.5 g soluble starch was added to 250 ml distilled water. The mixture was heated at 90 °C for approximately 10 min with constant stirring for the complete dissolution of soluble starch. The solution was then cooled to room temperature. Zinc nitrate hexahydrate, 7.44 g (0.025 mol) was added to the solution and then 250 ml of sodium hydroxide solution (0.2 mol/L) was added drop-wise with constant stirring. The transparent solution became milky white with no precipitation. The reaction continued for 2 h after adding NaOH. The solution was then centrifuged at 8000 rpm for 20 min, and the settled nano-ZnO was washed three times using distilled water to remove the salt and the excess soluble starch. The nano-ZnO was dried at 80 °C for 3 h to complete conversion of the remaining ZnOH to ZnO.

2.3. Preparation of GPS/nano-ZnO composites

Nano-ZnO particles were dispersed in a solution of distilled water (100 ml) and glycerol (1.5 g) and ultrasonicated for 1 h before adding 5 g pea starch. The nano-ZnO filler loading level (0, 0.5, 1, 2, 3 or 4 wt%) was based on the amount of pea starch. The mixture was heated at 90 °C for 0.5 h with constant stirring in order to plasticize the pea starch. To obtain the GPS/nano-ZnO composite films, the mixture was cast into a dish and placed in an air-circulating oven at 50 °C until dry (about 6–8 h).

2.4. Fourier-transform infrared spectroscopy (FT-IR)

FT-IR was performed on a Bio-Rad FTS3000 IR Spectrum Scanner.

2.5. Thermogravimetric analysis (TGA)

Thermal properties of the nano-ZnO and soluble starch powders were measured on a ZTY-ZP type thermal analyzer. Sample weight varied from 10 to 15 mg. Samples were heated from room temperature to 600 °C at a heating rate of 15 °C/min in a nitrogen atmosphere.

2.6. Transmission electron microscopy (TEM) and Scanning electron microscopy (SEM)

A suspension of nano-ZnO particles was dropped on a copper grid, then air-dried, and examined using a JEM-1200EX TEM. The GPS/nano-ZnO composites were cooled in liquid nitrogen, and then broken. The fracture surfaces were vacuum coated and examined using a Philips XL-3 scanning electron microscope.

2.7. Rapid visco analyser (RVA)

The pasting properties were analyzed using a rapid visco analyser (Newport Scientific, Sydney, Australia) according to AACC method 76-21 (Xie & Liu, 2004). Nano-ZnO particles were dispersed into a solution of distilled water (25 ml) and glycerol (0.375 g) then ultrasonicated for 1 h before adding 1.25 g of pea starch. The obtained starch slurry had the same composition as the mixture used for casting the GPS/nano-ZnO composites. The starch slurry was held at 50 °C for 1 min, then heated to 95 °C at 12.2 °C/min and held at 95 °C for 2.5 min. It was then cooled to 50 °C (cooling rate of 11.8 °C/min) and held at 50 °C for 2 min. The paddle speed was 960 rpm for 10 s and then decreased to 160 rpm for the remainder of the experiment.

2.8. Dynamic mechanical thermal analysis (DMTA)

The GPS/nano-ZnO composites for DMTA were stored in tightly sealed polyethylene bags for one week at 25 °C. DMTA was performed using a Mark Netzsch DMA242 analyzer operating at 1 Hz frequency. DMTA scans were performed between −80 and 120 °C with a heating rate of 3 °C/min.

2.9. Mechanical testing

The Testometric AX M350-10KN materials testing machine was operated with a crosshead speed of 50 mm/min for tensile testing (ISO 1184-1983 standard). The data were averaged over 6–8 specimens.

2.10. Ultraviolet–visible (UV–vis)

The UV–vis spectra of the GPS/nano-ZnO composites were recorded from 200 to 800 nm using a UV–vis spectrophotometer model U-1800, Hitachi Company.

2.11. Water vapor permeability (WVP)

WVP tests were carried out by ASTM method E96 (1996) with some modifications (Yu, Wang, & Ma, 2008). RH 0 was maintained using anhydrous calcium chloride in a cell. The composite films were cut into circles and sealed over the cell with melted paraffin. Each cell was stored in a desiccator containing saturated sodium chloride to provide a constant RH of 75% at 25 °C. WVP was determined by calculating the weight gain of the permeation cell. Changes in the weight of the cell were recorded as a function of time. Slopes were calculated by linear regression (weight change vs. time) and correlation coefficients for all reported data were >0.99. The water vapor transmission rate (WVTR) was defined as the slope (g/s) divided by the transfer area (m^2). After the permeation tests, film thickness was measured and WVP ($g\,Pa^{-1}\,s^{-1}\,m^{-1}$) was calculated as:

$$\mathrm{WVP} = \frac{\mathrm{WVTR}}{P(R_1 - R_2)} \cdot x \quad (1)$$

where P is the saturation vapor pressure of water (Pa) at the test temperature (25 °C), R_1 is the RH in the desiccator, R_2, the RH in the permeation cell and x is the film thickness (m). Under these conditions, the driving force $[P(R_1 - R_2)]$ is 1753.55 Pa.

3. Results and discussion

3.1. Characterization of nano-ZnO particles

As shown in Fig. 1a, the FT-IR spectra of bulk ZnO revealed a high intensity broad band at approximately 435 cm^{-1} resulting from the stretching of the zinc and oxygen bond. A similar band appeared in the nano-ZnO. In the fingerprint region of soluble starch, there were three characteristic peaks of –C–O– stretching. The peak at 1150 cm^{-1} was ascribed to C–O bond stretching of C–O–H group and two peaks at 1080 and 1016 cm^{-1} were attributed to C–O bond stretching of C–O–C group in the anhydroglucose ring of starch (Ma, Yu, & He, 2007). The peak at 2930 cm^{-1} was characteristic of the C–H stretching associated with ring methane hydrogen atoms (Fang & Fowler, 2002). The FT-IR spectra of nano-ZnO also recorded these peaks corresponding to soluble starch. The FT-IR spectra indicated that in the nano-ZnO particles there was strong binding, but no obvious formation of covalent bonds between soluble starch and ZnO.

The thermogravimetric (TG) and derivative thermogravimetric (DTG) curves of soluble starch and nano-ZnO are shown in Fig. 1b. The decomposed temperature appeared at a maximum rate of mass loss, i.e. the peak temperature shown in DTG curves. The decomposed temperature of soluble starch was 310.1 °C, while that of starch in nano-ZnO was 266.8 °C. Starch in nano-ZnO exhibited lower thermal stability than soluble starch. This could be attributed to the dissolution and heating of starch during the processing of nano-ZnO. The nano-ZnO showed a mass loss of 21 wt% at the decomposed temperature of starch. The quantity of starch in the nano-ZnO was calculated by matching the percentage of mass loss of nano-ZnO to the percentage of mass loss of soluble starch at the decomposed temperature (about 70 wt%). In this way, the content of starch in nano-ZnO was estimated to be about 30 wt%.

As shown in Fig. 1c1, aggregation of nano-ZnO particles of approximately 100 nm, was observed. The aggregates were comprised of nanocrystals of approximately 10 nm in size, as shown in Fig. 1c2. Both the aggregates and nano-ZnO particles were covered with starch. Since polysaccharides could form complexes with divalent metal ions, both of which were due to their high number of coordinating functional groups (hydroxyl and glucoside groups) (Taubert & Wegner, 2002), soluble starch could improve the stability of ZnO in water and prevent further aggregation of the ZnO, resulting in the formation of ZnO nanoparticles encapsulated by soluble starch in the preparation of ZnO nanoparticles.

3.2. SEM

As shown in Fig. 2a, no residual granules of pea starch were observed in the continuous GPS phase. At high temperature, water and glycerol physically break up the pea starch granules and disrupt inter- and intra-molecular hydrogen bonds making the pea starch plastic. The distribution of nano-ZnO particles in the matrix is shown in Fig. 2b and c. Nano-ZnO particles are dispersed evenly

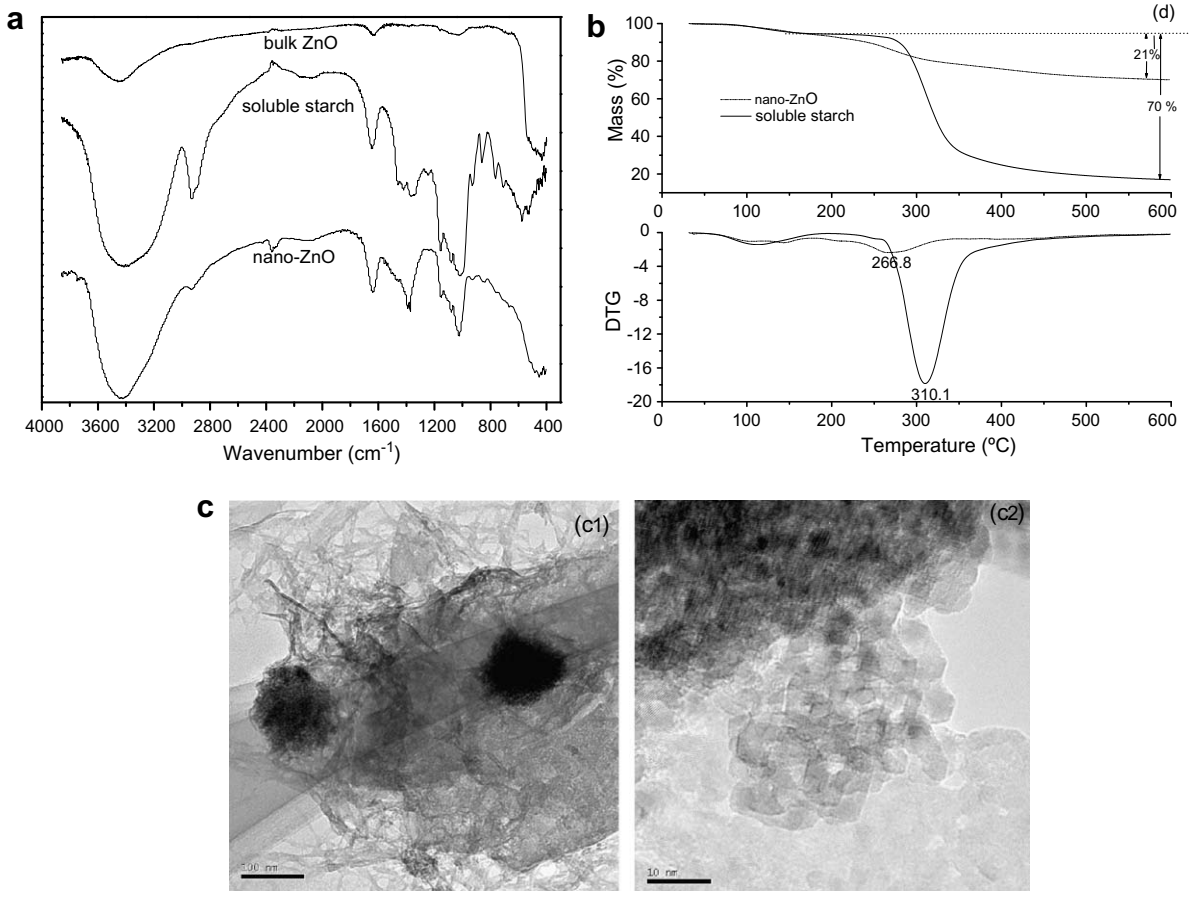

Fig. 1. (a) FT-IR of spectra of bulk ZnO, soluble starch and nano-ZnO, (b) thermogravimetric (TG) and derivative thermogravimetric (DTG) curves of soluble starch and nano-ZnO, TEM of nano-ZnO particles.

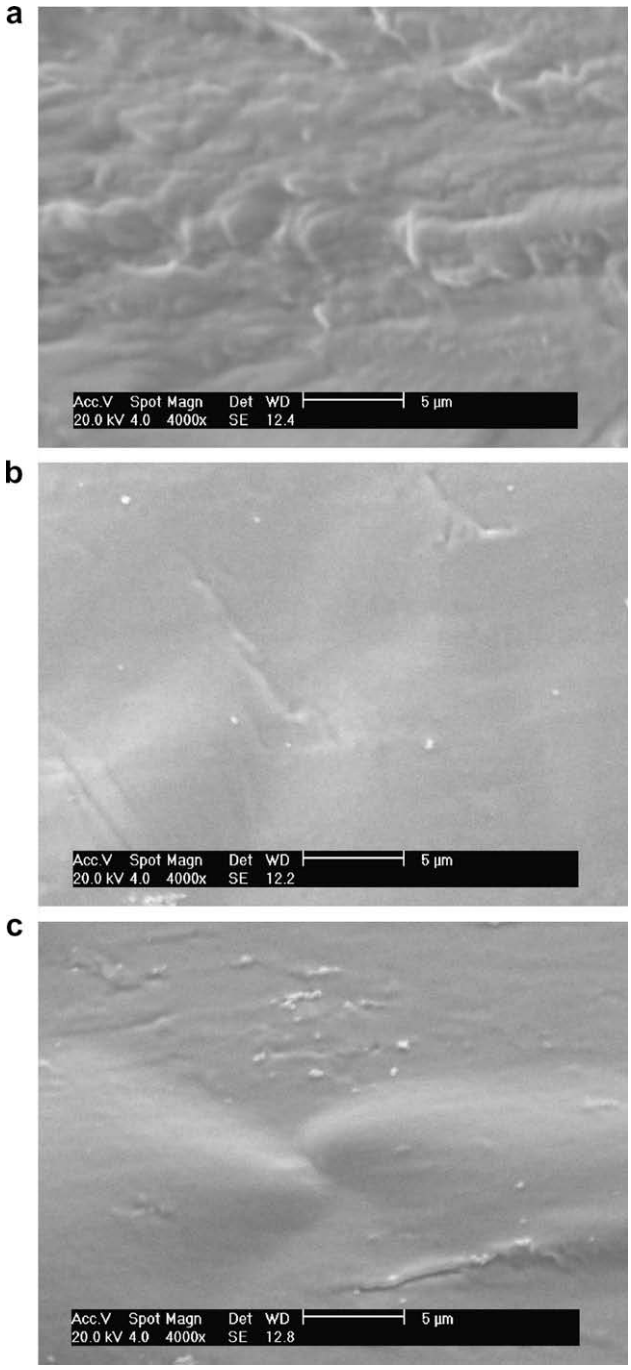

Fig. 2. SEM micrograph of the fracture surfaces of GPS/nano-ZnO composites. (a) 0 wt% nano-ZnO, (b) 1 wt% nano-ZnO, and (c) 3 wt% nano-ZnO.

in GPS matrix. A few agglomerates of nano-ZnO appeared in the GPS/nano-ZnO composites with higher nano-ZnO content.

3.3. RVA

The effect of nano-ZnO on the pasting properties of starch was studied by the rapid visco analyser, one of the most effective instruments with heating-cooling features (Fig. 3). In order to simulate the processing of GPS/nano-ZnO composites, a slurry identical to the casting solution was used in RVA analysis. When granular pea starch began to gelatinize in water, the viscosity increased and starch slurry turned into paste. Because nano-ZnO particles were

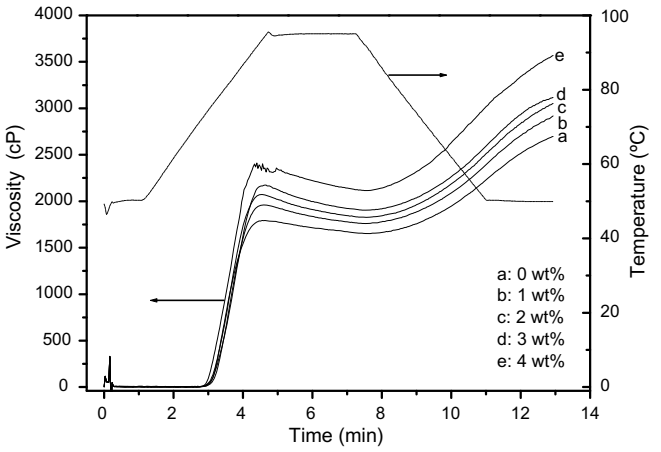

Fig. 3. Effect of nano-ZnO content on the viscometric profile.

encapsulated by soluble starch, the dispersion of nano-ZnO was more stable in the plasticized-starch solution than in the water. The interactions between the nano-ZnO and starch solution obviously increased the pasting viscosity when the nano-ZnO content increased a small amount of 1 wt% (about only 0.05 wt% of starch solution), as shown in Fig. 3.

3.4. DMTA

As shown in Fig. 4a, the storage modulus of GPS/nano-ZnO composites increased with the introduction of nano-ZnO particles. This improvement was likely due to the interaction between the GPS matrix and the nano-ZnO filler. Fig. 4b shows the curves for loss factor (tan delta) as a function of temperature for the nanocomposites. The loss factor was sensitive to molecular motion and its peak represents the glass transition temperature. The curve for GPS revealed two thermal transitions corresponding to the two separate phases in GPS. The upper transition (34.7 °C), occurred because of a starch-rich phase and was regarded as the glass transition temperature (T_g) of GPS materials. The lower transition, at −53.7 °C, was due to a starch-poor phase (Forssell & Mikkila, 1997). In GPS/nano-ZnO composites, both the upper and the lower transitions shifted to higher temperatures, indicating that both the starch-rich and starch-poor phases formed composites with nano-ZnO. The effect of nano-ZnO content on the upper transition however was more obvious than on the lower transition. The upper transition of the composites became higher with the increasing nano-ZnO content. Functioning like a physical joint, nano-ZnO improved the intermolecular interaction of GPS in the starch-rich phase, bringing adjacent chains of starch close, and reducing the free volume, thereby raising the T_g of composites as the nano-ZnO content increased.

3.5. Mechanical properties

Fig. 5 shows the effect of nano-ZnO content on the mechanical properties of GPS/nano-ZnO composites. As the filler in the GPS matrix, nano-ZnO exhibited an obvious reinforcing effect. As the nano-ZnO content increased, both the tensile yield strength and Young's modulus increased, but the elongation at break of the composites decreased. When the nano-ZnO content varied from 0 to 4 wt%, the tensile yield strength and Young's modulus increased, from 3.94 to 10.80 MPa and from 49.8 to 137.00 MPa respectively, while the elongation at break decreased from 42.2% to 20.4%. These changes relate to the interfacial interaction between nano-ZnO and GPS matrix.

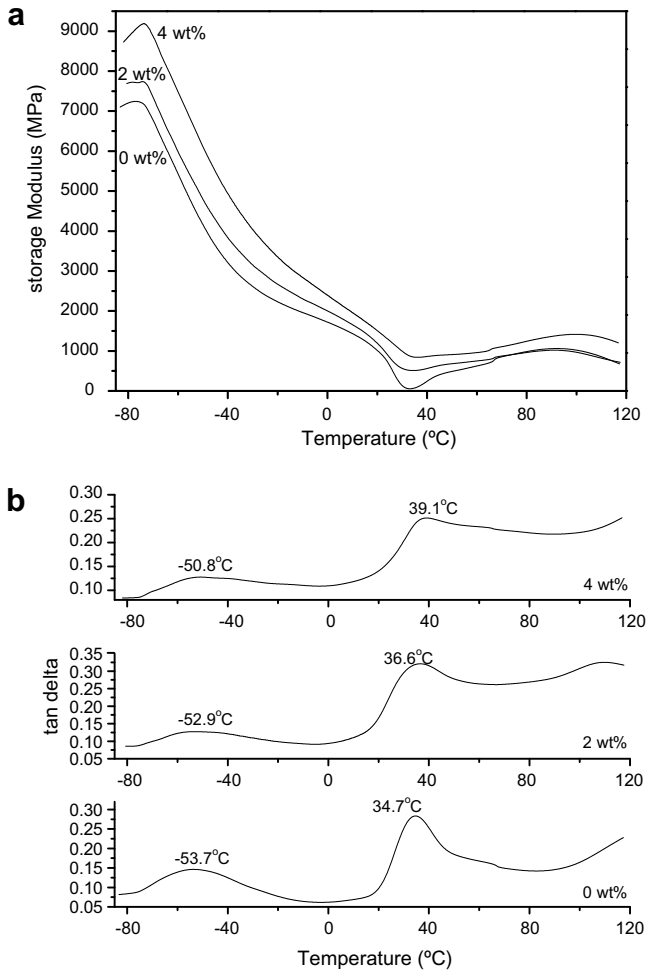

Fig. 4. Storage modulus (a) and tan delta (b) of GPS/nano-ZnO composite with different nano-ZnO content.

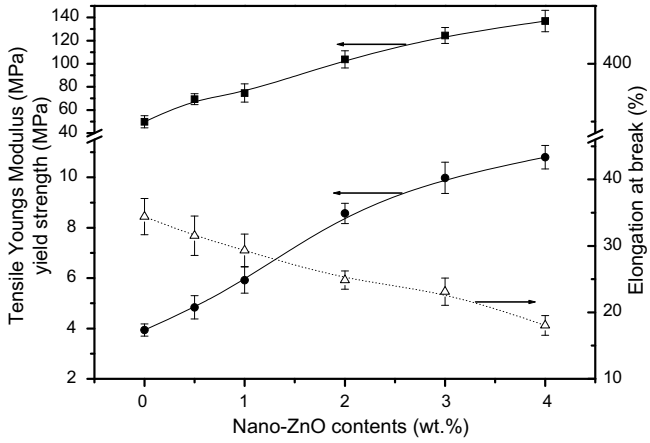

Fig. 5. Effect of nano-ZnO weight fraction on Young's modulus, tensile yield strength and elongation at break of GPS/nano-ZnO composites.

Interfacial interaction between the fillers and matrix was an important factor affecting the mechanical properties of the composites. Theoretical tensile yield strength of the composites was predicted using the Nicolais–Narkis model Eq. (2) (Metin, Tihminlioglu, Balkose, & Ulku, 2004) to estimate the adhesion between the filler particles and matrix,

$$\sigma_c = \sigma_m(1 - a\Phi_f^b) \quad (2)$$

where Φ_f, σ_c and σ_m are the volume fraction of the filler, and tensile yield strengths of the composite and matrix, respectively. In the Nicolais–Narkis model, parameters a and b are constants related to filler-matrix interaction and geometry of the filler, respectively. A value (a) of less than 1.21 represents good adhesion for composites containing spherical fillers. In the absence of adhesion for the composites, Eq. (2) became

$$\sigma_c/\sigma_m = (1 - 1.21\Phi_f^{2/3}) \quad (3)$$

This model was based on the assumption that the decrease in tensile strength was due to the reduction in effective cross-section area caused by spherical filler particles. If perfect adhesion between GPS and nano-ZnO particles occurred, the loading stresses would be transferred to the nano-ZnO, and no reduction in effective surface area would result.

The weight fraction of filler was converted to volume based on the densities of GPS and ZnO-soluble starch being 1.15 and 5.4 g/cm^3, respectively. Fig. 6 shows the experimental and theoretical curves plotted for the effect of the volume fraction on the yield stress ratio. The experimental values for the GPS/nano-ZnO composites were much higher than those calculated using Eq. (3) indicating a significant interaction between the GPS matrix and the nano-ZnO filler.

3.6. UV–vis

Fig. 7 shows the UV–vis absorbance of GPS/nano-ZnO composites with different levels of nano-ZnO content. An absorption peak appeared at 355 nm for GPS/nano-ZnO nanocomposites, while the peak in the bulk ZnO appeared at 380 nm (Vigneshwaran et al., 2006). The absorption peak of GPS/nano-ZnO composites exhibited an obvious blue-shift phenomenon due to the quantum confinement effect. With increasing nano-ZnO content, both the UV absorbance and the intensity of the absorption peaks increased. In the UV range (290–400 nm) pure GPS had very low absorbance, while the absorbance value peaked at 1.455 for the composite with 4 wt% nano-ZnO, meaning that the transmittance of UV light was only 3.51%, and most of UV light was shielded. The GPS/nano-ZnO nanocomposites may effectively protect against UV light, and could potentially be applied to UV-shielding materials.

3.7. WVP

Water vapor permeability (WVP) was used to study moisture transport through the film. As shown in Fig. 8, WVP of GPS/nano-

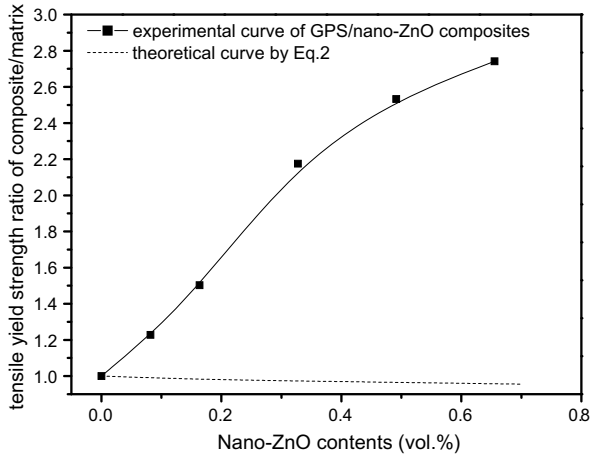

Fig. 6. Effect of nano-ZnO volume fraction on yield stress ratio of GPS/nano-ZnO composites.

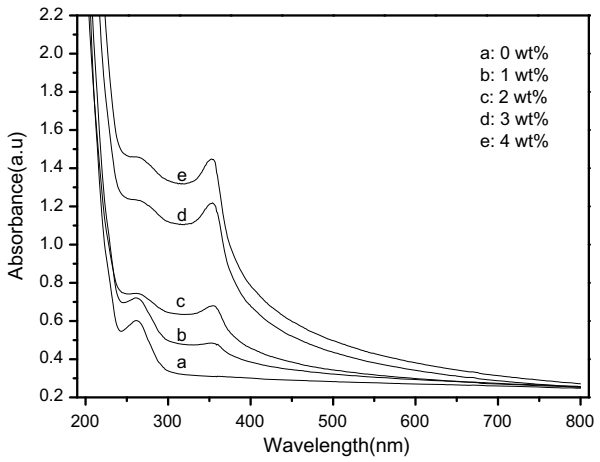

Fig. 7. UV–vis absorbance of GPS/nano-ZnO composites with different nano-ZnO contents.

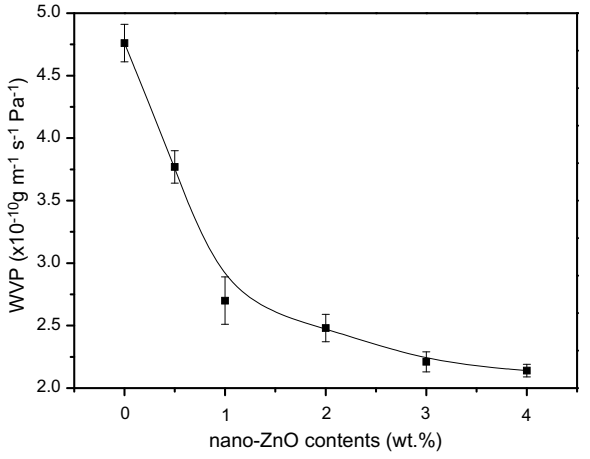

Fig. 8. Effect of nano-ZnO content on water vapor permeability of the composites.

ZnO composites decreased as the nano-ZnO content increased. Water vapor easily permeated the GPS film which had the highest WVP value, 4.76×10^{-10} g m^{-1} s^{-1} Pa^{-1}. As the nano-ZnO content increased, WVP values decreased significantly until the nano-ZnO content was 3 wt%, and then the values decreased only slightly (from 2.21×10^{-10} g m^{-1} s^{-1} Pa^{-1} at 3 wt% content to 2.18×10^{-10} g m^{-1} s^{-1} Pa^{-1} at 4 wt% content). Because the water resistance of nano-ZnO was better than that of the matrix, the addition of nano-ZnO probably introduced a tortuous path for water molecules to pass through (Kristo & Biliaderis, 2007). At the 3 wt% level, nano-ZnO dispersed well in the matrix with few paths for water molecules to pass through. As the nano-ZnO content increased to 4 wt%, the superfluous filler congregated easily, decreasing the effective content of filler and therefore had little effect on the decreasing of WVP.

4. Conclusion

GPS/nano-ZnO bionanocomposites were prepared by incorporating nano-ZnO particles into plasticized-starch. Soluble starch played a very important role not only in the stabilization of nano-ZnO but also in the fabrication of GPS/nano-ZnO composites. The strong interaction between nano-ZnO filler and the GPS matrix contributed to the improvement of bionanocomposite properties. At a low filler loading level (below 4 wt%), nano-ZnO enhanced the pasting viscosity, storage modulus, glass transition temperature, tensile yield strength and Young's modulus of GPS/nano-ZnO nanocomposites. Nano-ZnO impregnation also improved the absorbance of UV radiation and the water vapor barrier in comparison to pure GPS. These bionanocomposites have potential applications in medical, agricultural, drug release, packaging, and UV-shielding materials.

Acknowledgement

This work was financially supported in part by Agricultural Bioproducts Innovation Program (ABIP) of Canada via the Pulse Research Network (PURENet).

References

Angellier, H., Molina-Boisseau, S., & Dole, P. (2006). Thermoplastic starch-waxy maize starch nanocrystals nanocomposites. *Biomacromolecules, 7*, 531–539.

Bonnet, P., Albertini, D., & Bizot, H. (2007). Amylose/SWNT composites: From solution to film-synthesis, characterization and properties. *Composites Science and Technology, 67*, 817–821.

Cao, X. D., Chen, Y., & Chang, P. R. (2007). Preparation and properties of plasticized starch/multiwalled carbon nanotubes composites. *Journal of Applied Polymer Science, 106*, 1431–1437.

Cao, X. D., Chen, Y., Chang, P. R., Stumborg, M., & Huneault, M. A. (2008). Green composites reinforced with hemp nanocrystals in plasticized starch, *Journal of Applied Polymer Science,* doi:10.1002/app.28418.

Chandramouleeswaran, S., Mhaske1, S. T., Kathe, A. A., Varadarajan, P. V., Virendra, P., & Vigneshwaran, N. (2007). Functional behaviour of polypropylene/ZnO-soluble starch nanocomposites. *Nanotechnology, 18*, 385702–385709.

Darder, M., Aranda, P., & Ruiz-Hitzky, E. (2007). Bionanocomposites: A new concept of ecological, bio-inspired, and functional hybrid materials. *Advanced Materials, 19*, 1309–1319.

Fang, J. M., Fowler, P. A., & Tomkinson, J. (2002). The preparation and characterization of a series of chemically modified photo starches. *Carbohydrate Polymers, 47*, 245–252.

Forssell, P. M., & Mikkila, J. M. (1997). Phase and glass transition behaviour of concentrated barley starch–glycerol–water mixtures, a model for thermoplastic starch. *Carbohydrate Polymers, 34*, 275–282.

Huang, M. F., Yu, J. G., & Ma, X. F. (2005). High performance biodegradable thermoplastic starch – EMMT nanoplastics. *Polymer, 46*, 3157–3362.

Huang, M. F., Yu, J. G., & Ma, X. F. (2006). High mechanical performance MMT-urea and formamide-plasticized thermoplastic cornstarch biodegradable nanocomposites. *Carbohydrate Polymers, 63*, 393–399.

Kampeerapappun, P., Aht-Ong, D., Pentrakoon, D., & Srikulkit, K. (2007). Preparation of cassava starch/montmorillonite composite film. *Carbohydrate Polymers, 67*, 155–163.

Kristo, E., & Biliaderis, C. G. (2007). Physical properties of starch nanocrystal-reinforced pullulan films. *Carbohydrate Polymers, 68*, 146–158.

Lu, Y. S., Weng, L. H., & Cao, X. D. (2006). Morphological, thermal and mechanical properties of ramie crystallites – reinforced plasticized starch biocomposites. *Carbohydrate Polymers, 63*, 198–204.

Ma, X. F., Chang, P. R., & Yu, J. G. (2008). Electrically conductive carbon black (CB)/glycerol plasticized-starch (GPS) composites prepared by microwave radiation. *Starch/Starke, 60*, 373–375.

Ma, X. F., Yu, J. G., & He, K. (2007). The effects of different plasticizers on the properties of thermoplastic starch as solid polymer electrolytes. *Macromolecular Materials and Engineering, 292*, 503–510.

Ma, X. F., Yu, J. G., & Wang, N. (2007). Production of thermoplastic starch/mmt-sorbitol nanocomposites by dual-melt extrusion processing. *Macromolecular Materials and Engineering, 292*, 723–728.

Ma, X. F., Yu, J. G., & Wang, N. (2008). Glycerol plasticized-starch/multiwall carbon nanotube composites for electroactive polymers. , *Composites Science and Technology, 68*, 268–273.

Mangiacapra, P., Gorrasi, G., Sorrentino, A., & Vittoria, V. (2006). Biodegradable nanocomposites obtained by ball milling of pectin and montmorillonites. *Carbohydrate Polymers, 64*, 516–523.

Mathew, A. P., & Dufresne, A. (2002). Morphological investigation of nanocomposites from sorbitol plasticized starch and tunicin whiskers. *Biomacromolecules, 3*, 609–617.

Metin, D., Tihminlioglu, F., Balkose, D., & Ulku, S. (2004). The effect of interfacial interactions on the mechanical properties of polypropylene/natural zeolite composites. *Composites Part A, 35*, 23–32.

Park, H. M., Lee, W. K., & Park, C. Y. (2003). Environmentally friendly polymer hybrids – Part I – Mechanical, thermal, and barrier properties of thermoplastic starch/clay nanocomposites. *Journal of Materials Science, 38*, 909–915.

Taubert, A., & Wegner, G. (2002). Formation of uniform and monodisperse zincite crystals in the presence of soluble starch. *Journal of Materials Chemistry, 12*, 805–807.

Vigneshwaran, N., Kumar, S., & Kathe, A. A. (2006). Functional finishing of cotton fabrics using zinc oxide-soluble starch nanocomposites. *Nanotechnology, 17*, 5087–5095.

Xie, X. J., & Liu, Q. (2004). Development and physicochemical characterization of new resistant citrate starch from different corn starches. *Starch/Starke, 56*, 364–370.

Yu, J. G., Wang, N., & Ma, X. F. (2008). Fabrication and characterization of poly(lactic acid)/acetyl tributyl citrate/carbon black as conductive polymer composites. *Biomacromolecules, 9*, 1050–1057.

Zhao, X. P., Wang, B. X., & Li, J. (2008). Synthesis and electrorheological activity of a modified kaolinite/carboxymethyl starch hybrid nanocomposite. *Journal of Applied Polymer Science, 108*, 2833–2839.